Int. J. Heat Mass Transfer. Vol. 23, pp. 363–371
Pergamon Press Ltd. 1980. Printed in Great Britain

ION WIND ENHANCEMENT OF EVAPORATION INTO A LAMINAR AIR STREAM

F. X. HART and J. S. MASSEY
The Department of Physics, The University of the South, Sewanee, TN 37375, U.S.A.

(*Received* 2 *August* 1977 *and in revised form* 5 *June* 1979)

Abstract – The evaporation rate of a free liquid surface in a tangential, laminar air stream subjected to an ion wind is experimentally found to increase approximately as the square root of the current. The effect decreases with increasing flow rate and is greater for a positive ion wind than a negative. At a critical threshold current the laminar boundary layer is apparently destroyed. The evaporation rate then becomes governed by diffusion into a turbulent layer and is observed to increase more slowly with current. Except at the highest flow rates good agreement is obtained between experiment and numerical solutions of expressions obtained as approximations from the Navier–Stokes equations.

NOMENCLATURE

A, cross-sectional area of evaporation chamber;
b, parameter defined by equation (15);
c, vapor concentration in boundary layer;
c_0, vapor concentration at interface;
D, diffusion coefficient;
d, separation of needles from pan;
E, evaporation rate of water in ion wind;
E_0, control evaporation rate;
F, electric field;
f_x, electrical force in x direction;
f_y, electrical force in y direction;
$f(\eta)$, boundary layer profile function;
i, ion wind current;
i_0, threshold current for boundary layer disruption;
j, ion wind current density;
j_0, threshold current density;
K', electrode geometry factor in equation (6);
k, ionic mobility;
L, pan length;
M, molecular mass;
m, mass of water in pan;
n, exponent introduced in equation (15);
p, air pressure;
R, air flow rate;
Re, Reynolds number $= u_0/\nu x$;
T, absolute temperature;
t, time;
u, x component of air velocity in boundary layer;
u_0, free stream air speed;
u_e, equivalent free stream air speed for low flow rates;
V, applied voltage;
V_0, threshold voltage for corona discharge;
v, y component of air velocity in boundary layer;
W, pan width;
w, coordinate along pan width;
x, coordinate in direction of air flow;
y, coordinate normal to pan;
z, boundary layer compression;
$\hat{1}_y$, unit vector in y direction.

Greek symbols

δ, boundary layer thickness under ion wind;
δ_0, boundary layer thickness with no ion wind;
ε, permittivity;
ν, kinematic viscosity;
ρ, mass density;
ρ_c, charge density;
η, dimensionless coordinate scaling boundary layer;
η^*, dimensionless coordinate scaling boundary layer under ion wind.

1. INTRODUCTION

REPORTS of the enhancement of evaporation rates by electrostatic fields have appeared in the literature for many years [1, 2]. More recently, Sadek *et al.* [3] found that the drying rate of a horizontal surface in a tangential laminar air stream increased linearly with the voltage excess above corona onset; that is, as the square root of the ion wind current. Velkoff [4] and Kibler and Carter [5] showed theoretically and experimentally that heat transfer from a horizontal plate subjected to an ion wind from below increased as the fourth root of the current. Bologa and Rudenko [6] found significant evaporation rate increases from a free water surface for applied voltages above the threshold of corona current. The large increase in evaporation observed by Asakawa [7] might also be an ion wind effect [8] and thus vary as $i^{1/4}$.

The purposes of this paper are to derive from basic physical principles an expression for the evaporation rate of a liquid in a tangential laminar air flow subjected to an ion wind, to carefully determine experimentally the dependence of the evaporation increase on air flow rate, and to ascertain whether the applied field or current are responsible in part for the effect. Sadek *et al.* [3] used dimensional analysis to

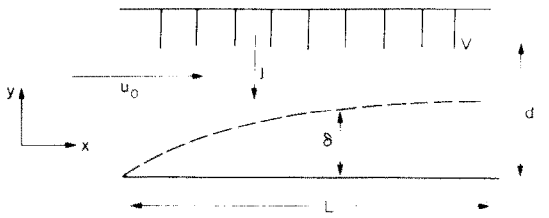

FIG. 1. Laminar boundary layer over pan. u_0 is the free stream air speed along the x axis. High voltage V applied to the needles set a distance d above the pan of length L produces an ion wind current j in the $-y$ direction. The resulting boundary layer thickness is δ.

obtain an expression for the drying rate as a function of applied voltage, whereas we begin with the Navier–Stokes equations and derive approximate expressions which are solved numerically to yield the velocity and concentration profiles in the boundary layer and the evaporation rate as functions of the ion wind current.

2. THEORY

Consider a pan of water in the x–w plane subjected to an air flow in the x direction with free stream speed u_0. As illustrated in Fig. 1, a high voltage V applied to an array of points set a distance d above the plane produces a current density j in the $-y$ direction. If u_0 is small a laminar boundary layer is formed over the pan. The warm air provides an energy input to drive the evaporation of water from the pan. At equilibrium the evaporation rate E of water from the pan is balanced by the rate of diffusion of the vapor through this layer

$$E(x,w) = -\mathrm{d}m/\mathrm{d}t = MD\partial c(x,y,w)/\partial y\big|_{y=0}, \quad (1)$$

where $-\mathrm{d}m/\mathrm{d}t$ is the time rate of change of the water's mass, M its molecular weight, D the diffusion coefficient of water vapor in air, and c the concentration of the vapor. Compression of the boundary layer by the applied current should thus increase the rate of diffusion and hence the evaporation rate.

Since variations in evaporation rate produced by the finite width of the pan are small [9], all w dependence may be neglected. The concentration gradient at the interface is found by solving the diffusion equation, which becomes under steady state conditions

$$D(\partial^2 c/\partial x^2 + \partial^2 c/\partial y^2) = u\partial c/\partial x + v\partial c/\partial y. \quad (2)$$

$u(x,y)$, $v(x,y)$ are, respectively, the x, y components of the air velocity in the boundary layer and may be found from the steady state Navier–Stokes equations in the x, y directions and the equation of mass conservation.

$$u\partial u/\partial x + v\partial u/\partial y = f_x/\rho - \rho^{-1}\partial p/\partial x + \nu(\partial^2 u/\partial x^2 + \partial^2 u/\partial y^2), \quad (3)$$

$$u\partial v/\partial x + v\partial v/\partial y = f_y/\rho - \rho^{-1}\partial p/\partial y + \nu(\partial^2 v/\partial x^2 + \partial^2 v/\partial y^2) \quad (4)$$

and

$$\partial u/\partial x + \partial v/\partial y = 0, \quad (5)$$

where p, ν, and ρ are respectively the pressure, kinematic viscosity and density of the air and f_x, f_y are respectively the x and y components of any force applied per unit volume of air. For an approximately constant temperature field the equation of energy may be neglected.

It should be noted that in the usual boundary layer approach the normal momentum equation is omitted. Since the ion wind current may introduce a significant normal component of momentum, the usual approach is here modified by retaining equation (4). The term 'boundary layer' is thus used here in a relaxed sense to refer to the layer of air immediately above the pan which diffusion limits the evaporation rate, rather than in the technical sense to imply that the normal component of momentum is neglected. The following analysis is then an approximate solution of the Navier–Stokes equations rather than an application of standard boundary layer theory.

When applied voltage V exceeds a threshold value V_0 at atmospheric pressure, an ion wind current given at small air flow speeds by [10]

$$i = K'kV(V - V_0), \quad (6)$$

begins to flow and space charge with density ρ_c is produced between the needle and pan. k is the ionic mobility and K' is a constant determined by the electrode geometry. The net electrical force exerted on a unit volume of air in this region is then [11]

$$\mathbf{f} = \rho_c\mathbf{F} + (8\pi)^{-1}\nabla(F^2\rho(\partial\varepsilon/\partial\rho)_T) - (8\pi)^{-1}F^2\nabla\varepsilon, \quad (7)$$

where $\mathbf{F}$ is the electric field, ε the permittivity and T the absolute temperature. If the medium is a gas the second and third terms on the right may be combined to yield

$$\mathbf{f} = \rho_c\mathbf{F} + (\varepsilon - 1)\nabla(F^2)/8\pi.$$

For air $\varepsilon \approx 1$ so that $\mathbf{f}_{\mathrm{air}} \approx \rho_c\mathbf{F}$. With water, a good electrical conductor, in the pan $F \approx 0$. For a poorly conducting liquid or a very thin interfacial region whose physical properties vary sharply but continuously from those of the gas to those of the liquid equation (7) would be required for a complete description of the net ponderomotive force. Since the evaporation rate of water is determined by diffusion in the gas phase, the existence of such a layer may be neglected.

Except near the edges of the array the horizontal components of the fields produced by the individual points cancel and $\mathbf{f}_y(y) = -\rho_c(y)F(y)\hat{\mathbf{l}}_y$ where $\hat{\mathbf{l}}_y$ is a unit vector in the y direction. Using $j = \rho_c kF$, one finds that the ion wind compressive force

$$f_y = -j/k, \quad (8)$$

is independent of y.

With no applied forces or pressure gradients in the

direction of flow, f_x and $\partial p/\partial x = 0$. Ion wind generated pressures are small in comparison to typical atmospheric pressures [12, 4], and furthermore we will assume that the pressure gradient in the direction normal to the plate is negligible. Hence, $\partial p/\partial y \approx 0$. Since velocity profile variations are much greater normal to the pan than along it, $\partial^2 u/\partial x^2 \ll \partial^2 u/\partial y^2$ and $\partial^2 v/\partial x^2 \ll \partial^2 v/\partial y^2$. Similarly, for concentration profiles $\partial^2 c/\partial x^2 \ll \partial^2 c/\partial y^2$

$$u\partial u/\partial x + v\partial u/\partial y = \nu\partial^2 u/\partial y^2, \tag{9}$$

$$u\partial v/\partial x + v\partial v/\partial y = -j/\rho k + \nu\partial^2 v/\partial y^2, \tag{10}$$

$$D\partial^2 c/\partial x^2 = u\partial c/\partial x + v\partial c/\partial y. \tag{11}$$

For $j = 0$ the problem reduces to simple flow along a flat plate. Equations (5) and (9) are solved simultaneously in the following way [13]. Note first that with $j = 0$ the normal momentum equation is omitted. The velocity profile in the boundary layer is expressed in terms of dimensionless coordinates. $u = u_0 f'(\eta)$ where $\eta = y(u_0/\nu x)^{1/2}$ and $'$ indicates differentiation with respect to η. Substitution in equation (5) yields $v = (u_0\nu/x)^{1/2}(\eta f'(\eta) - f(\eta))/2$. Equation (9) then becomes $2f''' + f''f = 0$ which may be solved numerically for the profile function $f(\eta)$ and thus $u(x, y)$ and $v(x, y)$. The boundary conditions are $f, f' = 0$ at $\eta = 0$ and $f' \to 1$ as $\eta \to \infty$. The boundary layer thickness δ_0, defined as the height above the plate at which $u = 0.99u_0$, is found to occur at $\eta = 4.84$.

The simplicity of the above approach is essentially due to the scaling of the boundary layer in terms of the Reynolds number $Re = u_0/\nu x$. A solution of these equations when $j = 0$ should incorporate u_0, ν and x only in Re. Pohlhausen [14] solved the equation for heat transfer from a flat plate by expressing it in dimensionless form in terms of η and using the above numerical solutions for u and v. The similarity of the heat transfer and diffusion equations indicates that this approach is also applicable to simple mass transfer for $j \neq 0$.

We modify this procedure for the situation where $j = 0$ by letting $\eta^* = y(u_0/\nu x)^{1/2}/b$ be a new dimensionless coordinate. b is a dimensionless parameter which incorporates the ion wind compression of the boundary layer. To preserve similarity b cannot depend explicitly on u_0, ν, x or y. The velocity profile in the boundary layer is expressed as

$$u = u_0 f'(\eta^*). \tag{12}$$

Substitution of (12) into (5) yields

$$v = b(u_0\nu/x)^{1/2}(\eta^* f'(\eta^*) - f(\eta^*))/2 \tag{13}$$

and equation (9) becomes

$$2f'''/b^2 + f''f = 0, \tag{14}$$

which may be solved numerically for $f(\eta^*)$.

As the ion wind current density is increased, the boundary layer thickness decreases until it disappears at j_0. The appearance of very low amplitude waves on the water surface is an indication that this value has been exceeded. At the other extreme, the results found for simple flow along a flat plate must be obtained as $j \to 0$. These limiting case conditions may be met by letting

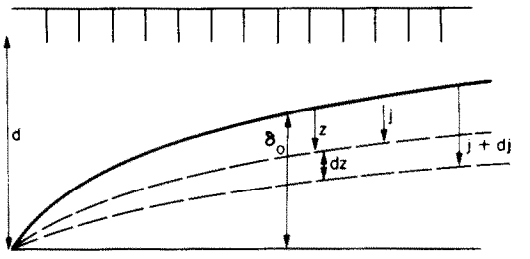

FIG. 2. Compression of the boundary layer by the ion wind. δ_0 is the original thickness. A current density j compresses the layer by an amount z, a density $j + dj$ by $z + dz$. d is the height of the needles above the pan.

$$b = 4.84(1 - (j/j_0)^n) \tag{15}$$

and using as boundary conditions for (14): $u, v = 0$ at $\eta^* = 0$ and $u = 0.99u_0$ at $\eta^* = 1$. The ion wind compressed boundary layer thickness becomes then

$$\delta = 4.84(1 - (j/j_0)^n)(\nu x/u_0)^{1/2} = \delta_0(1 - (j/j_0)^n).$$

Up to this point the normal momentum equation has not been used and the approach thus parallels that of standard boundary layer theory. Equation (10) is now introduced to obtain a value for n and an expression for j_0. Consider the force exerted by the ion wind current on a unit volume of air at the top of the boundary layer as illustrated in Fig. 2. z is a coordinate in the $-y$ direction such that $z = 0$ at the top of the boundary layer for $j = 0$. Application of the current compresses the boundary layer by an amount z. If the viscous force exerted by the air in the free stream is neglected, a unit volume of air is accelerated from rest in the vicinity of the needles by a net force $f_y = -j/k$. At the top of the boundary layer it has acquired a downward velocity given by $v^2 = 2d' f_y/\rho$ where $d' = d - \delta_0 + z$ is the distance from the needles to the top of the boundary layer. Hence

$$v = (2j(d - \delta_0 + z)/\rho k)^{1/2}. \tag{16}$$

With the use of equations (12) and (13) equation (10) may be expressed at the top of the boundary layer where $\eta^* = 1$ and $f' \approx 1$ as

$$b_j \nu^{1/2}(u_0/x)^{3/2}(f_j(1) - 1 - f_j(1)f_j''(1))/4 = -j/\rho k + \nu\partial^2 v/\partial z^2\big|_z. \tag{17}$$

$f_j(1)$ and $f_j''(1)$ are respectively the boundary layer profile function and its second derivative for an applied current j evaluated at the top of the boundary layer ($\eta^* = 1$). If the current density is increased slightly to $j + dj$, the boundary layer is compressed to $z + dz$ and equation (10) becomes

$$b_{j+dj}\nu^{1/2}(u_0/x)^{3/2}(f_{j+dj}(1) - 1 - f_{j+dj}(1)f_{j+dj}''(1))/4 = -(j + dj)/\rho k + \nu\partial^2 v/\partial z^2\big|_{z+dz}. \tag{18}$$

Retention of the first order in a Taylor expansion of the kinematic viscosity term on the right hand side and subtraction of equation (17) from (18) leads to

$$\nu^{1/2}(u_0/x)^{3/2}(b_{j+dj}f_{j+dj}(1) - b_jf_j(1) - (b_{j+dj} - b_j) - (b_{j+dj}f''_{j+dj}(1)f_{j+dj}(1) - b_jf''_j(1)f_j(1)))/4 = -\mathrm{d}j/\rho k + \nu\partial^3 v/\partial z^3\big|_z \mathrm{d}z. \quad (19)$$

Equations (19) and (14) form a set of coupled, nonlinear differential equations which describe in detail the modification of the boundary layer by the ion wind, but whose complexity prevents a straightforward solution. An approximate solution may be found by assuming that a small change in current density does not produce a significant change in either the value of f at the top of the layer ($f_j(1) \approx f_{j+dj}(1)$ and $f''_j(1) \approx f''_{j+dj}(1)$) or of b_j ($b_j \approx b_{j+dj}$). The latter implies that the exponent in equation (15) is small. The errors introduced by this approximate solution will be discussed later. The left side of equation (19) then vanishes, the differential equations are decoupled, and we have $\mathrm{d}j/\rho k = \nu \mathrm{d}^3 v/\mathrm{d}z^3\big|_z \mathrm{d}z$. Differentiation of equation (16) yields

$$\mathrm{d}j/j^{1/2} = 3\nu(2\rho k)^{1/2}\mathrm{d}z/8(d - \delta_0 + z)^{5/2},$$

which may be integrated to obtain

$$j^{1/2} = (2\rho k)^{1/2}\nu(1 - (1 + z/(d - \delta_0))^{-3/2})/8(d - \delta_0)^{3/2}.$$

This equation may be inverted to yield the boundary layer compression z as a function of the current density j.

$$1 + z/(d - \delta_0) = (1 - j^{1/2}8(d - \delta_0)^{3/2}/\nu(2\rho k)^{1/2})^{-2/3}.$$

Keeping only first order terms in an expansion of the right side leads to

$$z = 16(d - \delta_0)^{5/2}j^{1/2}/3\nu(2\rho k)^{1/2}. \quad (20)$$

This simple expression is valid for $j^{1/2}$ sufficiently small that the higher order terms dropped in the expansion of the preceding equation are negligible. In equation (15) we may set $n = 1/2$ with the expectation that serious deviations should appear for

$$j \approx \rho k\nu^2/32(d - \delta_0)^3. \quad (21)$$

According to equation (20) greater boundary layer compression and hence greater evaporation should occur for greater separation of the pins above the pan (d) and smaller ionic mobility (k).

An expression for the threshold current for boundary layer disappearance may be found from equation (20) by noting that disappearance corresponds to a compression of $z = \delta_0$ or

$$j_0 = 9\delta_0^2\rho k\nu^2/128(d - \delta_0)^5. \quad (22)$$

It should be noted, however, that the higher order terms dropped in the expansions leading to equations (19) and (20) may no longer be neglected for thin boundary layers. Hence the values for j_0 predicted using equation (22) are of questionable validity.

Substitution of equations (12) and (13) into (11) yields an expression for $c(\eta^*)$

$$2Dc''/\nu b^2 + fc' = 0, \quad (23)$$

which may be solved numerically under the boundary conditions $c = c_0$ at $\eta^* = 0$ and $c = 0.01c_0$ at $\eta^* = 1$.

The evaporation rate from a strip of width W at a distance x from the leading edge of the pan is then

$$E(x) = WMD(u_0/\nu x)^{1/2}c'(0)/b.$$

The rate of mass loss from the entire pan is found by integrating the above expression from 0 to L to obtain

$$\mathrm{d}m/\mathrm{d}t = -2DMW(Lu_0/\nu)^{1/2}c'(0)/b. \quad (24)$$

If the variation of j_0 with ν and δ_0 is formally

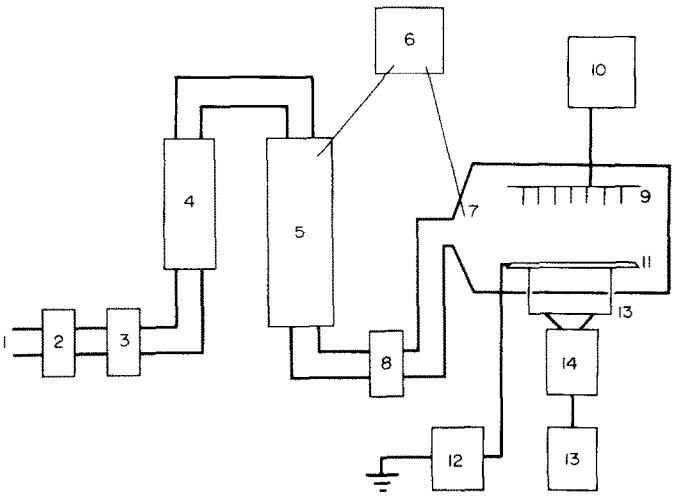

FIG. 3. Block diagram of the apparatus. (1) Compressed air enters system, (2) drying chamber, (3) coarse particle filter, (4) flowmeter, (5) heating tube, (6) temperature controller, (7) temperature probe at entrance to evaporation chamber, (8) fine particle filter, (9) needles, (10) high voltage supply, (11) pan with water, (12) electrometer, (13) plexiglass spacer, (14) pan balance, (15) recorder.

suppressed and j_0 is regarded simply as a parameter of the system, the boundary layer remains scaled according to Re. In practice this is indeed the case since j_0 must be determined experimentally. Each value of j then determines a new value of b and different solutions of equations (14) and (23). The ion wind enhancement of evaporation rate in equation (24) is contained explicitly in b, which decreases as $j^{1/2}$ in equation (15), and implicitly in $c'(0)$, which is obtained by numerical solution of equations (14) and (23).

3. EXPERIMENTAL

Figure 3 is a block diagram of the apparatus used to measure the evaporation rate of water exposed to an ion wind current of known density for several boundary layer thicknesses. A stream of compressed air passes through a drying and coarse filtering system in to a Matheson Model 620 flowmeter where its rate may be adjusted to an accuracy of 3%. The air next enters a long tube where it is heated by passage over a nichrome coil. The current through the coil is adjusted by a Yellow Springs Model 72 proportional temperature controller so that the temperature of the air at the entrance of the evaporation chamber is maintained to within 0.2°C of a pre-selected value (28.0°C). From the tube the air passes through a Gelman Type A glass fiber filter which removes at least 98% of all particles larger than 0.05 μm.

The upper electrode is a rectangular array of Milwards No. 1 embroidery needles with a separation of approximately 3 cm. High voltage is supplied to it by a Spellman Model RHR60PN30 bipolar power supply. The resulting ion wind current passes through the water to ground via a fine wire and a Keithley Model 602 electrometer. The water is contained in a rectangular pan ($34.5 \times 18.5 \times 0.7$ cm) whose bottom is coated with wax to prevent the addition of impurities to the water from the metal. The pan rests on a plexiglass spacer which, in turn, is supported by a Mettler Model PE-1200 balance whose analytic output is sent to an Esterline Angus Model E1102E recorder.

The boundary layer thickness, which may be varied by changing the flow rate, is found experimentally from the temperature profile, determined with a thermocouple, of the air stream above the pan.

At the start of a run, deionized water (resistivity of the order of 10^6 ohms cm^{-3}) maintained at a temperature of 17°C is added to fill the pan. Approximately 20 min are allowed for thermal equilibrium to be established and for a monolayer to form. The surface is then carefully skimmed with tissue to remove any such film. The water is now permitted to evaporate with no applied voltage. The recorded decrease in mass with time furnishes the control evaporation rate E_0. High voltage is then applied to the needles and adjusted to produce a pre-selected ion wind current. The recorded decrease in mass with time furnishes the current enhanced evaporation rate E. After the high voltage is removed, a final evaporation rate is obtained in order to assess the importance of evaporative cooling of the surface. No attempt is made to directly control the temperature of the water during the evaporation run since this would interfere with the monitoring of the ion wind current. Because the chamber cannot be completely isolated from its surroundings, its temperature varies slightly with that of the room. For a given air flow setting, however, the evaporation rate is quite reproducible. The per cent standard deviation ranges from 6% for the lowest flow rate to 2% for the highest.

The threshold current for wave production is determined by visual observation of the water surface. These results may be checked by photographing the image of a brightly illuminated checkerboard pattern reflected from the water surface. Photographs taken for several different current densities of either polarity are inspected for the presence of waves.

4. RESULTS

The evaporation rate from the pan with no applied current may be calculated using equation (24) with $j = 0$ and then compared to the observed control rate as a test of the model. In that equation u_0 is the free stream air speed above a fully developed laminar boundary layer. For the highest flow rates used in the experiment the temperature profiles indicate that the boundary layer thicknesses are small in comparison to the separation of the needles from the pan. The free stream air speed is approximately equal to the average air speed. Hence $u_0 \approx R/A$ where R is the air flow rate in cm^3 s^{-1} and A is the cross-sectional area of the chamber (250 cm^2). For low flow rates, however, the temperature profiles indicate a merging of the boundary layers beneath the pin supports and above the pan. An equivalent free stream air speed u_e may be found by setting the average air speed R/A equal to the average speed in the laminar boundary layer above a flat plate $\langle u \rangle$. Since $u = u_e f'(\eta^*)$

$$\langle u \rangle = \int_0^1 u \, d\eta^* \Big/ \int_0^1 d\eta^* = u_e f(1)$$

or $u_e = R/Af(1)$. Numerical solution of equation (14) indicates that $f(1) \approx 0.65$ for the lower flow rates used in the experiment.

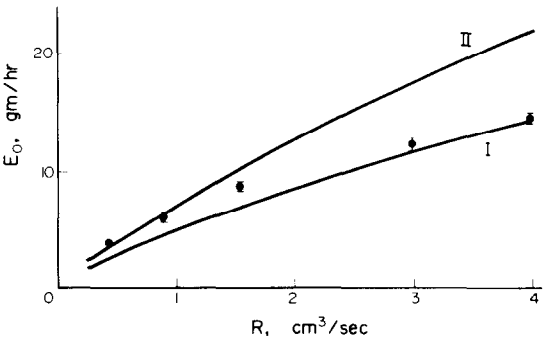

FIG. 4. Control evaporation rate E_0 for several air flow settings R. Values calculated from equation (24) are plotted as line I using u_0 and as line II using u_e. Experimental values are plotted with error bars.

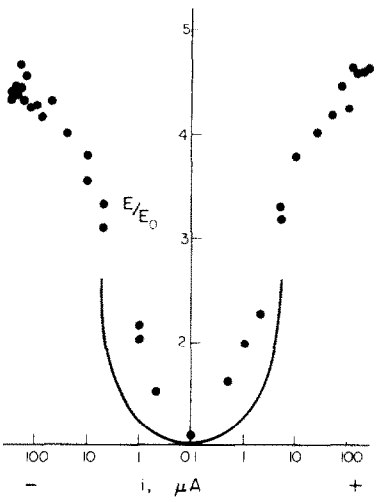

FIG. 5. Ratio of evaporation rate in ion wind to control rate vs ion wind current for lowest flow setting, $R = 450\,\text{cm}^3\,\text{s}^{-1}$.

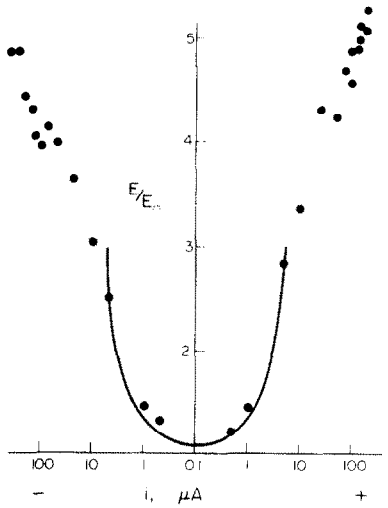

FIG. 6. Ratio of evaporation rate in ion wind to control rate vs ion wind current for $R = 910\,\text{cm}^3\,\text{s}^{-1}$.

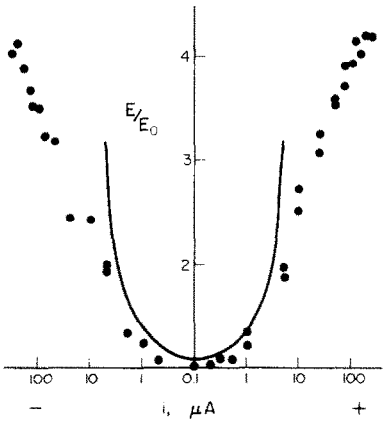

FIG. 7. Ratio of evaporation rate in ion wind to control rate vs ion wind current for $R = 1550\,\text{cm}^3\,\text{s}^{-1}$.

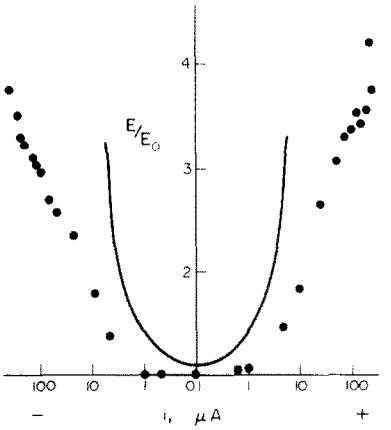

FIG. 8. Ratio of evaporation rate in ion wind to control rate vs ion wind current for $R = 3000\,\text{cm}^3\,\text{s}^{-1}$.

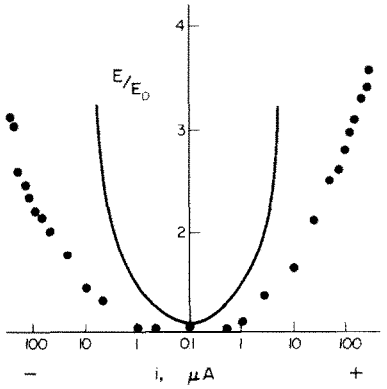

FIG. 9. Ratio of evaporation rate in ion wind to control rate vs ion wind current for highest flow setting, $R = 4000\,\text{cm}^3\,\text{s}^{-1}$.

Table 1. Evaporation ratios at three positive and negative current levels for each flow setting

R ($\text{cm}^3\,\text{s}^{-1}$)	i (μA)	$(E/E_0)_+$	$(E/E_0)_-$
450	1	1.98	2.15
	10	3.78	3.66
	100	4.24	4.26
910	1	1.45	1.47
	10	3.35	3.04
	100	4.86	3.95
1550	1	1.33	1.23
	10	2.72	2.42
	100	3.94	3.50
3000	1	1.06	1.00
	10	1.83	1.78
	100	3.37	2.96
4000	1	1.10	1.04
	10	1.63	1.44
	100	2.79	2.45

For each flow rate the surface temperature of the water is measured by a thermocouple and the corresponding vapor pressure found in a handbook [15]. Equation (24) is then solved numerically according to the procedure described above with $D = 0.25\,\mathrm{cm^2\,s^{-1}}$, $M = 18 \times 1.67 \times 10^{-24}\,\mathrm{g}$ and $\nu = 0.15\,\mathrm{cm^2\,s^{-1}}$. Figure 4 compares the average, experimentally determined control rate for each flow setting with the rate calculated from equation (24) using $u_0 = R/A$ (line I) and $u_e = R/Af(1)$ (line II). The length of the error bars is twice the standard deviation of the experimentally determined rate. The experimental rates agree very well with the rates predicted using u_0 for the higher flow settings and u_e for the lower.

The ratio of the evaporation rate with an applied current to the control rate during the same run, E/E_0, is plotted against the applied current i for five flow settings in Figs. 5–9. The experimental values are indicated by dots. In each case the evaporation rate increases sharply at first with applied current and more gradually at higher currents. Table 1, which lists for each flow setting the experimentally determined evaporation ratios at three positive and negative ion wind current levels, indicates that the enhancement of evaporation by the applied current is reduced as the air flow rate increases. Note also that with the possible exception of the lowest flow setting, for a given current evaporation is increased more by a positive ion wind than by a negative.

The solid lines in Figs. 5–9 are the evaporation ratios calculated using equation (24). For reasons to be discussed later the threshold current for boundary layer disappearance used in that expression is taken to be $10\,\mu\mathrm{A}$ ($j_0 = 1.8 \times 10^{-8}\,\mathrm{A\,cm^{-2}}$) for each flow setting. In each case the shape of the theoretical curve is quite similar to the course of the experimental points below $5\,\mu\mathrm{A}$. Furthermore, good agreement is obtained between the calculated evaporation ratios and those determined experimentally for the three lower flow settings. Serious differences appear, however, between the experimental and calculated ratios at the two highest flow settings.

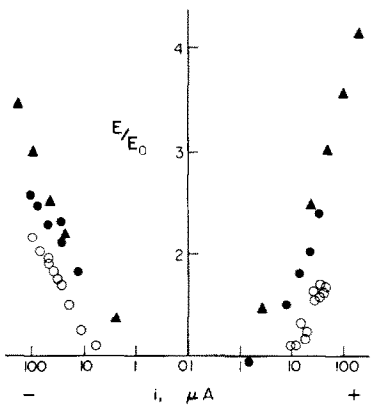

FIG. 10. Ratio of evaporation rate with corona discharge to control rate vs corona current. Solid circles correspond to discharge from guard ring wires with $R = 450\,\mathrm{cm^3\,s^{-1}}$, open circles with $R = 1610\,\mathrm{cm^3\,s^{-1}}$. The solid triangles represent the current to a screen placed above the boundary layer.

Several tests may be performed to investigate whether the evaporation increases are produced at least in part by the electric field or current flow rather than the ion wind *per se*. A sheet of metal screening (0.68 cm mesh) is erected 1.35 cm above the water's surface and grounded through a microammeter. At the highest flow setting the boundary layer above the water is almost entirely confined beneath the screen as confirmed by the measured temperature profile. High voltage applied to the needles results in a large ion wind current to the screen but not to the water. In addition, the boundary layer is shielded from the field by the screening.

Figure 10 illustrates the evaporation ratios obtained in two of the experiments performed to confirm the ion wind model. Large increases in evaporation are observed with the presence of the screen. Moreover, waves are readily generated on the water surface even though it is not exposed to any current flow or electric field. The ion wind generated between the needles and screen passes through the screen and can disrupt the boundary layer.

To test whether the strong inhomogeneous electric field in the vicinity of the needles affects the evaporation rate, a large choking resistor is added in series between the needles and the high voltage supply. When the potential difference between the needles and pan reaches the level of corona onset, a large voltage drop is produced across the resistor and the discharge is quenched. At a sufficiently high voltage output from the power supply a corona can be sustained from the needles in addition to the large voltage drop across the choking resistor. For applied voltages less than this value no increase in evaporation is observed. Once this value is exceeded small increases in evaporation, consistent with the corresponding ion wind current effects previously obtained, are found.

To investigate the reported [2] increase in evaporation in a uniform field the needles are replaced by a very smooth, plane upper electrode separated 2.72 cm from the water surface. For voltages up to breakdown (23 kV) no increase in evaporation is observed. It should be added that initial experiments with this configuration had shown a significant increase. A metal sheet had been installed as a guard ring around the pan to ensure uniformity of the field over the water. Measurement of the current to ground through the guard ring indicated that a corona discharge was being generated from the edge of the guard ring at those voltages which were apparently producing an increase in evaporation. Application of corona dope to the edges eliminated the discharge and the evaporation increase. Three short, fine wires were then installed at the front edge of the guard ring. When the applied voltage was sufficiently high to produce corona from the wire tips the evaporation rate of the water increased markedly as indicated in Fig. 10. As before, the enhancement of evaporation is reduced by an

increase in flow rate. The boundary layer upstream from the pan is evidently disrupted by the discharge and undergoes a gradual transition from laminar to turbulent. A similar effect has been described by Velkoff and Ketcham [16]. The increased evaporation in a uniform field observed by Miura [2] may be attributed to corona from the edges of his electrodes.

5. DISCUSSION

As noted previously, qualitative agreement between the shape of the predicted curve and the course of the experimental points is achieved for all flow settings and good absolute agreement is obtained except for the two highest flow settings. Better results can be attained at these settings if j_0 in equation (15) is increased with flow rate rather than taken to be a constant in the calculations. The threshold current should not be obtained in practice from equation (22) since, as noted previously, the validity of that equation is questionable. Moreover, in that equation j_0 depends very critically on the original boundary layer thickness at the place where the layer disappears. The low level corona discharge from the needles is not uniform and often appears to be concentrated at a few sources which vary in position as the needle tips are conditioned by the discharge. Hence the point at which the boundary layer first disappears varies with time.

The threshold current densities obtained visually and photographically are used for j_0 in equation (15). Visual values range between 7 and 12 μA while at least 10 μA are required to produce a noticeable distortion in the photographically obtained pattern. Any observable dependence of j_0 on flow rate was masked by fluctuations in the point of discharge and thus the original boundary layer thickness. For this reason the threshold current is taken to be 10 μA ($j_0 = 1.8 \times 10^{-8}$ A cm^{-2}) for all flow rates in the calculation.

Although the value for j_0 obtained from equation (22) could not be actually used in the calculations, its magnitude may be compared with the observed threshold current as a rough test of the model. For the medium flow rate, positive ions ($k = 1.8$ cm^2 V^{-1} s^{-1}), and $\rho = 1.2 \times 10^{-3}$ g cm^{-3}, $j_0 = 1.1 \times 10^{-8}$ A cm^{-2} which is in reasonable agreement with the observed value.

Some error is introduced by the evaporative cooling of the water's surface. The enhanced evaporation produced by the ion wind cools the water and lowers the saturation vapor pressure. The observed evaporation rate is then reduced below that which would be obtained if the surface were maintained at constant temperature. Measurement of a control evaporation rate immediately after the high voltage is switched off indicates that the decrease in evaporation rate amounts to only a few per cent. Similarly the error introduced by the absence of a well defined free stream air speed at low flow rates is also small.

The major sources of error are the inability to accurately predict the threshold current for all flow rates and the simplifying assumptions made in obtaining equations (19) and (20). The first leads to the necessity of using the same experimentally determined value for j_0 for all flow rates whereas j_0 apparently increases with air speed. The second restricts consideration to small currents and changes in boundary layer thickness. Deviations from the predicted values are thus expected as $j \to j_0$.

At high current levels the increase in evaporation rate becomes more gradual. Local disruptions in the laminar boundary layer propagate downstream causing the eventual destruction of the entire laminar layer. Generation of waves by the ion wind causes mass loss due to spraying and further disturbances in the boundary layer [17]. The observed evaporation rates are still small in comparison with those predicted by kinetic theory for evaporation from a free surface and thus must be limited by diffusion into a turbulent layer above the wavy surface. The more gradual rise in the evaporation rate at high current levels evidently corresponds to the gradual transition from a laminar to a fully turbulent boundary layer over the surface.

The greater increase in evaporation caused by positive ions noted in Table 1 is expected from equation (20). Typical positive ion mobilities in humid air are about 20–40% lower than negative mobilities [18]. Hence positive ions, being less mobile, should produce a greater compression of the boundary layer than negative ions for the same current density.

The dependence of evaporation rate on ion wind current is quite complicated in tangential laminar flow and cannot be fully characterized by a simple functional relationship. An approximate relationship can be obtained from equation (1) by assuming a linear concentration profile so that

$$\partial c/\partial y\,|_{y=0} \approx c_0/\delta = c_0/\delta_0(1 - (i/i_0)^{1/2}).$$

Thus

$$E/E_0 \approx (1 - (i/i_0)^{1/2})^{-1} \approx 1 + (i/i_0)^{1/2}/2.$$

It is instructive to compare the results in the present study to those reported elsewhere regarding the ion wind enhancement of heat and mass transfer. The present study finds an approximate $i^{1/2}$ dependence for evaporation into a laminar air stream which is similar to the results reported by Sadek *et al.* [3] and shows that the effect decreases with increasing flow rate. Bologa and Rudenko [6] do not explicitly graph evaporation rate vs ion wind current, but a log–log plot of the data contained in their Fig. 2 indicates an increase as $V^{3/2}$ (approximately as $i^{3/4}$) for evaporation originally governed by free convection. It should be noted, however, that the presence of waves on their free water surface indicates turbulence in the air above the surface. Kibler and Carter [5] and Velkoff [4] have shown that the heat transfer from a plate is increased as $i^{1/4}$ by an ion wind directed from below. Similarity implies that mass transfer under the same conditions should vary in the same way. It is clear that the ion wind enhancement of heat and mass

transfer cannot be summarized in a simple current dependence, but rather depends critically on the particular flow pattern of the system. Further studies should be carried out to investigate the interaction of an ion wind with turbulent boundary layers and with slowly moving air streams where the effects of both free and forced convection are important.

Acknowledgements – We would like to express our appreciation to Dr. Wayne Holman for his translation of Ref. [6], to Mr. Ralph James for his assistance with the experimental work, and to Dr. Basil Antar for his helpful suggestions. This study has been supported by a grant from the Research Corporation.

REFERENCES

1. J. R. Sutton, A contribution to the study of evaporation from water surfaces, *Sci. Proc. R. Dublin Soc.* **11,** 137–178 (1907).
2. A. Miura, Investigation of evaporation in the electric field, *Science Reports Tohuku Univ. Ser.* 5 **5,** 160–162 (1953).
3. S. F. Sadek, R. G. Fax and M. Hurwitz, The influence of electric fields on convective heat and mass transfer from a horizontal surface under forced convection, *Trans. ASME Ser.* C **94,** 144–148 (1972).
4. H. R. Velkoff, Electro-fluid mechanics: investigation of the effects of electric fields in heat transfer and boundary layers, ASD-TDR-62-650, AF Aero-Propulsion Laboratory, Wright-Patterson AFB, Ohio, pp. 11, 44–50 (1962).
5. K. G. Kibler and H. G. Carter, Electrocooling in gases, *J. appl. Phys.* **45,** 4436–4440 (1974).
6. M. K. Bologa and V. M. Rudenko, Acceleration of liquid evaporation by applying an electric field, *Elektron. Obrab. Mater.* **3,** 37–40 (1975).
7. Y. Asakawa, Promotion and retardation of heat transfer by electric fields, *Nature* **261,** 220–221 (1976).
8. K. G. Kibler and H. G. Carter, Heat transfer with electric fields, *Nature* **264,** 295 (1976).
9. D. R. Davies and T. S. Walters, Further experiments on evaporation from small, saturated plane areas into a turbulent boundary layer, *Proc. Phys. Soc. B* **65,** 640–645 (1952).
10. S. Chapman, Corona point current in wind, *J. geophys. Res.* **75,** 2165–2169 (1970).
11. L. D. Landau and E. M. Lifshitz, *Electrodynamics of Continuous Media,* p. 68. Addison-Wesley, Reading (1960).
12. A. P. Chattock, On the velocity and mass of the ions in the electric wind in air, *Phil. Mag.* **48,** 401–420 (1899).
13. H. Schlichting, *Boundary-Layer Theory,* 6th ed., pp. 117–131. McGraw-Hill, New York (1968).
14. E. Pohlhausen, Heat transfer between solid bodies and fluids with negligible friction and thermal conductivity, *Z. angew. Math. Mech.* **1,** 115–121 (1921).
15. *Handbook of Chemistry and Physics,* 40th ed., pp. 2325–2326. Chemical Rubber Co., Cleveland (1958).
16. H. R. Velkoff and J. Ketcham, Effect of an electrostatic field on boundary layer transition, *AIAA Jl* **6,** 1381–1383 (1968).
17. E. P. Anisimova, G. E. Kononkova, V. V. Kuznetsov, A. S. Orlov, G. I. Popov and A. A. Speranskaya, Wind–wave generation and the wind velocity structure in the air above a wavy water surface, *Boundary-Layer Meteorol.* **6,** 5–11 (1974).
18. H. Israel, *Atmospheric Electricity,* Vol. 1, 2nd ed., pp. 142–143. Israel Program for Scientific Translation, Jerusalem (1970).

ACCROISSEMENT PAR VENT D'IONS DE L'EVAPORATION DANS UN ECOULEMENT LAMINAIRE D'AIR

Résumé — L'évaporation d'une surface liquide libre, dans un écoulement d'air tangentiel, laminaire, soumis à un vent d'ions, est trouvée expérimentalement accrue approximativement comme la racine carrée du courant. L'effet décroit avec la vitesse croissante de l'écoulement et il est plus grand pour un vent d'ions positifs que négatifs. Pour un courant critique, la couche limite laminaire est apparamment détruite. Le flux d'évaporation est alors gouverné par la diffusion dans une couche turbulente et il croît plus lentement avec le courant. Sauf pour les vitesses les plus grandes on obtient un bon accord entre l'expérience et la solution numérique obtenues à partir de l'équation de Navier–Stokes.

DURCH IONENWIND UNTERSTÜTZTE VERDUNSTUNG IN EINEM LAMINAREN LUFTSTROM

Zusammenfassung—Die Verdunstungsrate einer freien Flüssigkeitsoberfläche in einem tangentialen laminaren Luftstrom unter dem Einfluß eines Ioenewindes nimmt — wie Versuche gezeigt haben — annähernd mit der Quadratwurzel des Stromes zu. Die Wirkung nimmt bei stärkerer Strömung ab und ist bei positivem Ionenwind größer als bei negativem. Anscheinend wird bei einer kritischen Stromschwelle die laminare Grenzschicht zerstört. Die Verdunstungsrate wird dann von der Diffusion in eine turbulente Schicht beherrscht, und man beobachtet nur eine leichte Zunahme mit steigendem Strom. Außer bei den höchsten Strömungsgeschwindigkeiten läßt sich eine gute Übereinstimmung zwischen Experiment und numerischen Lösungen von Ansätzen erhalten, die näherungsweise von den Navier–Stokes-Gleichungen hergeleitet wurden.

ИНТЕНСИФИКАЦИЯ ИСПАРЕНИЯ В ЛАМИНАРНЫЙ ПОТОК ВОЗДУХА ЗА СЧЕТ ИОННОГО ВЕТРА

Аннотация — Экспериментально найдено, что при наличии ионного ветра интенсивность испарения со свободной поверхности жидкости в тангенциальный ламинарный поток воздуха увеличивается почти пропорционально квадратному корню из тока. Влияние ионного ветра уменьшается с увеличением скорости течения; положительные ионы оказывают большее влияние, чем отрицательные. Вероятно, что при критическом пороговом токе ламинарный пограничный слой разрушается. При этом интенсивность испарения определяется диффузией в турбулентный слой и с увеличением тока возрастает более медленно. За исключением случая очень больших скоростей течения наблюдается хорошее соответствие между экспериментальными и численными решениями уравнений, полученных в приближении уравнений Навье–Стокса.